PNAS RESEARCH ARTICLE | CELL BIOLOGY OPEN ACCESS

The TOR complex controls ATP levels to regulate actin cytoskeleton dynamics in *Arabidopsis*

Liufeng Dai[a], Baojie Wang[a], Ting Wang[a], Etienne H. Meyer[b], Valentin Kettel[b], Natalie Hoffmann[c], Heather E. McFarlane[c], Shalan Li[d], Xuna Wu[d], Kelsey L. Picard[e,f], Patrick Giavalisco[g], Staffan Persson[e,h,i,j], and Yi Zhang[a,k,1]

Edited by Roberto Zoncu, University of California, Berkeley; received December 22, 2021; accepted July 28, 2022 by Editorial Board Member Rebecca Heald

Energy is essential for all cellular functions in a living organism. How cells coordinate their physiological processes with energy status and availability is thus an important question. The turnover of actin cytoskeleton between its monomeric and filamentous forms is a major energy drain in eukaryotic cells. However, how actin dynamics are regulated by ATP levels remain largely unknown in plant cells. Here, we observed that seedlings with impaired functions of target of rapamycin complex 1 (TORC1), either by mutation of the key component, *RAPTOR1B*, or inhibition of TOR activity by specific inhibitors, displayed reduced sensitivity to actin cytoskeleton disruptors compared to their controls. Consistently, actin filament dynamics, but not organization, were suppressed in TORC1-impaired cells. Subcellular localization analysis and quantification of ATP concentration demonstrated that RAPTOR1B localized at cytoplasm and mitochondria and that ATP levels were significantly reduced in TORC1-impaired plants. Further pharmacologic experiments showed that the inhibition of mitochondrial functions led to phenotypes mimicking those observed in *raptor1b* mutants at the level of both plant growth and actin dynamics. Exogenous feeding of adenine could partially restore ATP levels and actin dynamics in TORC1-deficient plants. Thus, these data support an important role for TORC1 in coordinating ATP homeostasis and actin dynamics in plant cells.

TOR | energy | actin | cytoskeleton

Significance

Cells must overcome energy shortage, and the ability to do so determines their fate. The ability of cells to coordinate their cellular activities and energy status is therefore important for all living organisms. One of the major energy drains in eukaryotic cells is the constant turnover of the actin cytoskeleton, which consumes ATP during the cycle of polymerization and depolymerization. We report that the TOR complex, a master regulatory hub that integrates cellular energy information to coordinate cell growth and metabolism, controls cellular ATP levels in plant cells. We further elucidate that low ATP levels cause reduced actin dynamics in plant cells. These findings provide insight into how plant cells handle low energy situations.

Energy is essential for all fundamental physiological processes in a living organism. Energy deficiency elicits diverse responses that allow cells to overcome the challenge of energy starvation and therefore dictate whether a cell will survive or die (1). One of the more energy-costly processes in cells is the dynamic turnover of the actin cytoskeleton, which plays vital roles in cell mobility, cell division, cell polarity establishment and maintenance, and cell morphogenesis (2–4). The function of the actin cytoskeleton relies on its dynamic rearrangement, including assembly of actin monomers into filaments of various architectures and disassembly of these structures back into monomers (5). During cycles of actin assembly and disassembly, actin monomers polymerize into filaments in an adenosine triphosphate (ATP)-bound state, and the polymerization of actin is followed by the irreversible hydrolysis of ATP to adenosine diphosphate (ADP) and phosphate (6). After ATP hydrolysis, phosphate dissociates from polymerized actin, leaving ADP-actin in the filaments. Depolymerization of actin filaments then releases ADP-actin monomer back into the cytoplasm, where ADP is rapidly exchanged for ATP, restarting the cycle. The cost of ATP by actin turnover is particularly high in plant cells, as actin filaments in the cortical arrays of plant cells grow at rates 10 to 100 times faster than the actin filaments in fission yeast or in the dendritic actin array at the leading edge of motile metazoan cells (7). The high growth rate of actin filaments is balanced by the disassembly of filaments through severing activity, resulting in fast-growing but short-lived actin filaments in plant cells (8). The incredible dynamics of actin filaments allow plant cells to rapidly respond to constantly changing environments, but at the expense of high amounts of ATP (9). Despite the undisputed importance of ATP for actin cytoskeleton remodeling, little is known about how ATP levels affect actin dynamics in plant cells.

Target of rapamycin (TOR), an evolutionary conserved serine/threonine protein kinase in eukaryotes, is a master regulatory hub that integrates cellular information about nutrient and energy availability to coordinate cell growth and metabolism (10–13). In yeast and mammalian cells, TOR acts as the catalytic subunit in at least two structurally and functionally distinct multiprotein complexes, referred to as TOR complex 1 (TORC1) and TORC2, respectively (14). With the lethal with SEC13 protein 8 (LST8) being a common component in both TORC1 and TORC2, the two

Author contributions: P.G., S.P., and Y.Z. conceived the project; L.D. and Y.Z. designed research; L.D., B.W., T.W., E.H.M., V.K., S.L., X.W., and K.L.P. performed the experiments; N.H. and H.E.M. performed the immuno-TEM experiments; L.D. and Y.Z. analyzed the data; and L.D. and Y.Z. wrote the paper with input from all of the authors.

The authors declare no competing interest.

This article is a PNAS Direct Submission. R.Z. is a guest editor invited by the Editorial Board.

Copyright © 2022 the Author(s). Published by PNAS. This open access article is distributed under Creative Commons Attribution-NonCommercial-NoDerivatives License 4.0 (CC BY-NC-ND).

[1]To whom correspondence may be addressed. Email: yi.zhang@bnu.edu.cn.

This article contains supporting information online at http://www.pnas.org/lookup/suppl/doi:10.1073/pnas.2122969119/-/DCSupplemental.

Published September 12, 2022.

complexes are defined by the presence of their signature subunits: regulatory-associated protein of TOR (RAPTOR) for TORC1 and rapamycin-insensitive companion of TOR (RICTOR) for TORC2 (15, 16). The core subunits of TORC1, TOR, RAPTOR, and LST8 have been identified in plants, implying the existence of a plant TORC1 (17–19). By contrast, TORC2-specific components are not conserved in plants (20–22). A single copy of TOR and two homologs of RAPTOR (RAPTOR1A and RAPTOR1B) are present in the genome of *Arabidopsis thaliana* (18, 23). While mutants of the lowly expressed *RAPTOR1A* are indistinguishable from wild-type (WT) plants under standard growing conditions, the mutation of *RAPTOR1B* leads to a wide range of phenotypes similar to the ones observed after the inhibition of *TOR* expression or activity (18, 24, 25). Thus, RAPTOR1B seems to act as the major RAPTOR isoform in *Arabidopsis* TORC1.

Along with other functions, TORC2 regulates actin cytoskeleton organization, likely via Rho signaling and AGC family protein kinases, in yeast and mammalian cells (15, 16, 26, 27). Despite the absence of plant TORC2, a functional link between TOR and actin cytoskeleton was proposed in plant cells. Through a genetic screen for mutants with defects in vacuole morphogenesis, a recent report identified *eva1*, a mutant of *isopropylmalate synthase 1* (*IPMS1*) that encodes a critical enzyme for Leu biosynthesis (28). This mutant contained increased levels of branched-chain amino acids (BCAAs). The characterization of *eva1* and other *ipms1* mutant alleles revealed that BCAA overaccumulation led to the up-regulation of TOR activity and actin filament bundling in *Arabidopsis* cotyledon epidermal cells (28). Actin bundling was compromised when exogenous BCAA was fed to plants with reduced expression of TOR. However, this was not the case in WT plants and in *raptor1b* mutants, indicating that a functional TOR, but perhaps not RAPTOR, is required for the reorganization of actin filaments induced by the overaccumulation of BCAAs (28). Nevertheless, how TOR regulates actin cytoskeleton dynamics under normal growth conditions and whether RAPTOR participates in this regulatory mechanism remain elusive. In this report, we show that TOR and RAPTOR1B affect cellular ATP levels, which is necessary to maintain actin dynamics, but not its organization.

Results

Seedlings with Impaired TORC1 Functions Display Reduced Sensitivity to Actin Inhibitors. To decipher molecular mechanisms that underlie actin maintenance, we undertook a forward genetic screen to identify mutants that were less sensitive to the specific and membrane-permeable inhibitor for actin polymerization, Latrunculin B (LatB). We used the homozygous SALK T-DNA collections of *Arabidopsis* (29) for the screen and grew seedlings from those lines on media supplemented with LatB for 6 days in the dark. We found that seedlings of one of the lines, SALK_022096, affecting *RAPTOR1B* [*rb22*; *rb* for *raptor1b*, followed by the first two nonzero digits of the SALK line number, as in Salem et al. (30)], had longer etiolated hypocotyls compared to WT seedlings. To confirm these results, we regrew the progeny of *rb22* and three additional independent T-DNA mutants of *RAPTOR1B* [*rb10,* SALK_101990; *rb78*, SALK_078159; *rb64*, SALK_006431; Zhang et al. (25)] on LatB-containing media and on media containing cytochalasin D (CD), another specific actin cytoskeleton disruptor, respectively. The etiolated *rb* mutant hypocotyls were significantly shorter than WT under control conditions, indicating cell elongation defects in the mutants (Fig. 1*A* and *C*). However, all *rb* mutant seedlings were less sensitive than WT to LatB and CD, displaying less swollen hypocotyls (Fig. 1*B*). Quantitative analysis confirmed that the application of actin inhibitors markedly inhibited hypocotyl growth in WT seedlings and that the hypocotyl lengths of *rb* mutants were less affected by these inhibitors (Fig. 1*C* and *D*). Consistently, light-grown *rb* mutants displayed reduced sensitivity to LatB treatment, resulting in less inhibited primary root length in the presence of LatB (*SI Appendix*, Fig. S1*A* and *B*). By contrast, oryzalin, an inhibitor disrupting microtubule polymerization, suppressed hypocotyl elongation in *rb* mutants to an extent similar to that in the WT (*SI Appendix*, Fig. S2*A* and *B*).

RAPTOR1B is a component of TORC1, which plays central roles in the stimulation of cell growth and metabolism in response to nutrients (12, 20, 31). We therefore tested whether the core protein of TORC1, the TOR kinase itself, participated in controlling the sensitivity of seedlings to LatB. Similar to the *rb* mutants, impairment of TOR function, either by genetically knocking down the expression level of *TOR* (32, 33) or by inhibiting TOR activity using the previously described inhibitors AZD8055 and Torin2 (34–36), resulted in significantly reduced sensitivity to LatB (Fig. 1*E*–*G*). These data suggest that TOR and RAPTOR1B, most likely as a complex, negatively regulate the sensitivity of seedlings to actin disruptors.

Impairment of TORC1 Functions Causes Decreased Actin Cytoskeleton Dynamics. To examine the organization of actin cytoskeleton, we crossed a fluorescent marker of actin filaments, mNeonGreen-fABD2, into the two *rb* mutants, *rb10* and *rb64*, respectively. In parallel, we also assessed the effects of TOR inhibitors on actin filament organization. We focused the analysis in the epidermal cells from the dark-grown hypocotyls, as this cell type has been used as a model cell type for imaging actin arrays with high spatial and temporal resolution (7, 8). The organization of actin filaments in *rb* mutants and AZD8055-treated Col-0 plants resembled that of WT seedlings under normal growth conditions (Fig. 2*A*). The amount of actin filaments (as quantified by fluorescent density) and the bundling of actin filaments [as quantified by skewness (37)] did not show significant differences in *rb* mutants and AZD8055-treated plants compared to their controls (Fig. 2*B* and *C*). By contrast, the effect of LatB on actin filaments was diminished in the *rb* mutants and AZD8055-treated plants compared to their controls, which resulted in significantly increased amounts of actin filaments remaining in these plants after LatB treatment (Fig. 2*D* and *E*). These observations indicated that actin filaments may be stabilized in *rb* mutants and AZD8055-treated plants.

To investigate actin filament dynamics, we collected time-lapse images of mNeonGreen-fABD2 by spinning disk confocal microscopy. The global actin filament dynamics were first investigated through a correlation coefficient analysis (38). This analysis quantified the extent of overall actin filament rearrangements over time by calculating the correlation of fluorescent intensity at all pixel positions between all pairwise temporal intervals. The change in actin organization over time was reflected by the rate of decay of correlation coefficient values as the temporal interval increased. The correlation coefficient curves decayed significantly slower in *rb* mutants and TOR inhibitor-treated cells compared to the control (Fig. 2*F*–*H* and *SI Appendix*, Fig. S3*A* and *B*). Similarly, short-term AZD8055 treatment caused significantly reduced rates of decay of correlation coefficient values compared to the control (*SI Appendix*, Fig. S3*C* and *D*). These data indicated that actin filament dynamics were attenuated when TORC1 activity was inhibited in plant cells.

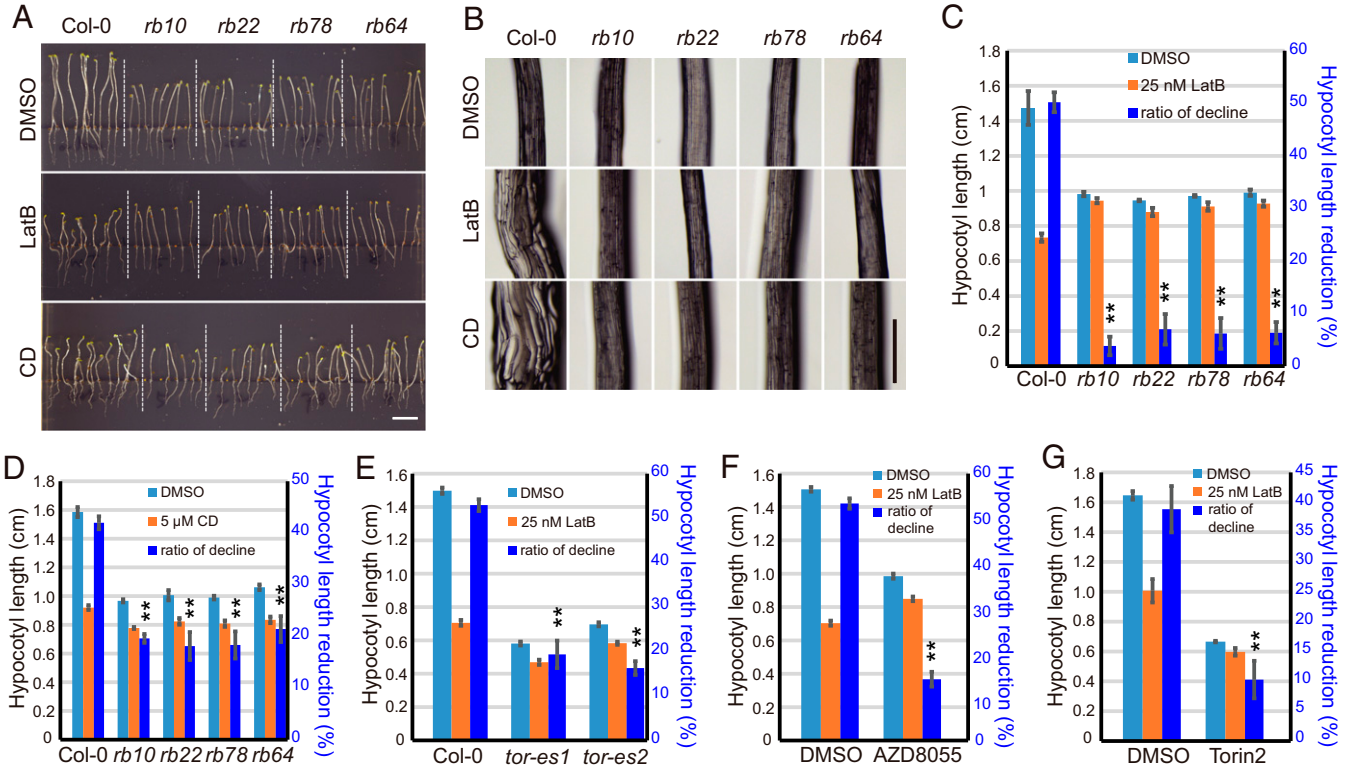

Fig. 1. Inhibition of TORC1 functions affected plant sensitivity to actin cytoskeleton inhibitors. (*A*) Six-day-old Col-0, *rb10*, *rb22*, *rb78*, and *rb64* seedlings grown in the dark on half MS media (*Upper Panel*), on half MS media supplemented with 25 nM LatB (*Center Panel*) or 5 μM CD (*Lower Panel*). Scale bar, 5 mm. (*B*) Close-up of hypocotyl cells in (*A*) using stereomicroscopy. Scale bar, 500 μm. (*C* and *D*) Bar graphs of hypocotyl length grown on media supplemented with LatB (*C*) or CD (*D*). Blue bars show the ratios of hypocotyl length reduction caused by actin inhibitors. (*E*) Hypocotyl length of Col-0 and two estradiol-inducible *TOR-RNAi* lines [*tor-es1* and *tor-es2*; see Xiong and Sheen (33)] grown on media supplemented with estradiol and LatB. Blue bars show the ratios of hypocotyl length reduction caused by actin inhibitors. (*F* and *G*) Hypocotyl length of Col-0 plants grown on media supplemented with LatB in the absence or presence of TOR inhibitor AZD8055 (*F*) or Torin2 (*G*). Blue bars show the ratios of hypocotyl length reduction caused by actin inhibitors. Values in (*C*) to (*G*) are means ± SEs from 3 biological replicates with more than 10 seedlings per replicate. The double asterisk indicates that the ratio of hypocotyl length reduction caused by actin inhibitors is significantly different compared to the control by Student's *t* test; $P < 0.01$.

We next analyzed individual actin filament dynamics by quantifying actin filament behaviors (8). Actin filament dynamics are dominated by rapid elongation and the disappearance of filaments due to the high frequency of filament severing in the *Arabidopsis* cortical arrays (8). The filament elongation rate and severing frequency were significantly reduced in both *rb* mutants and AZD8055-treated plants compared to their controls (Fig. 2*I*), corroborating that the impairment of TORC1 functions led to reduced actin filament dynamics. In agreement with these observations, a significant increase in filament lifetime was observed in *raptor1b* mutants and AZD8055-treated plants compared to their controls (Fig. 2*I*).

To further compare the polymerization rate of actin filaments, we performed washout experiments. A high concentration of LatB was applied to completely depolymerize actin filaments, and then the inhibitor was washed out by moving plants to media without LatB. The restoration of actin filaments was significantly slower in *rb* mutants and AZD8055-treated plants compared to their controls (Fig. 2*J* and *K*), indicating an inhibited polymerization rate of actin filaments.

To assess actin filament dynamics in the presence of LatB, the correlation coefficient analysis was performed after short-term treatment with the inhibitor. A moderate concentration of LatB was applied to avoid excessive depolymerization of actin filaments. The correlation coefficient curves decayed significantly slower after the application of LatB compared to the control, suggesting that LatB treatment reduced actin filament dynamics (*SI Appendix*, Fig. S4*A*). However, the effects of LatB were ameliorated in *rb* mutants (*SI Appendix*, Fig. S4*B*), further implying a reduced sensitivity to LatB in these plants.

Altogether, these data suggested that actin filaments adopted a decreased dynamic remodeling pattern in TORC1-impaired cells, thus establishing a new balance of actin remodeling to maintain an actin organization similar to WT.

GFP (Green Fluorescent Protein)-RAPTOR1B Localizes at Mitochondria in Plant Cells. The subcellular localization of TOR and related components has not been carefully examined, and little is therefore known regarding where the TORC1 works in plant cells. To examine the subcellular localization of RAPTOR1B and hence deduce its possible function, we generated two fluorescently tagged RAPTOR1B constructs under the control of its native promoter, *pRAPTOR1B::EGFP-RAPTOR1B* and *pRAPTOR1B::mNeonGreen-RAPTOR1B*, and transformed them into *rb10* and *rb22* mutant plants, respectively. The constructs were functional as they restored growth and sensitivity to LatB of the *rb* mutants (*SI Appendix*, Fig. S5*A*, *B*, *D*, and *E*). In addition, TOR activity and its response to glucose supply were rescued in the complementation line, as indicated by the elevated phosphorylation levels of the conserved substrate S6K1 of TOR at Thr^{449} in the protoplast transient expression assay (32) (*SI Appendix*, Fig. S5*C*).

We observed GFP signals in cytosol and cytosolic compartments (Fig. 3*A*–*J*). To determine to which compartments GFP-RAPTOR1B is localized, we introgressed red fluorescent protein (RFP)-, mCherry-, or cyan fluorescent protein (CFP)-tagged

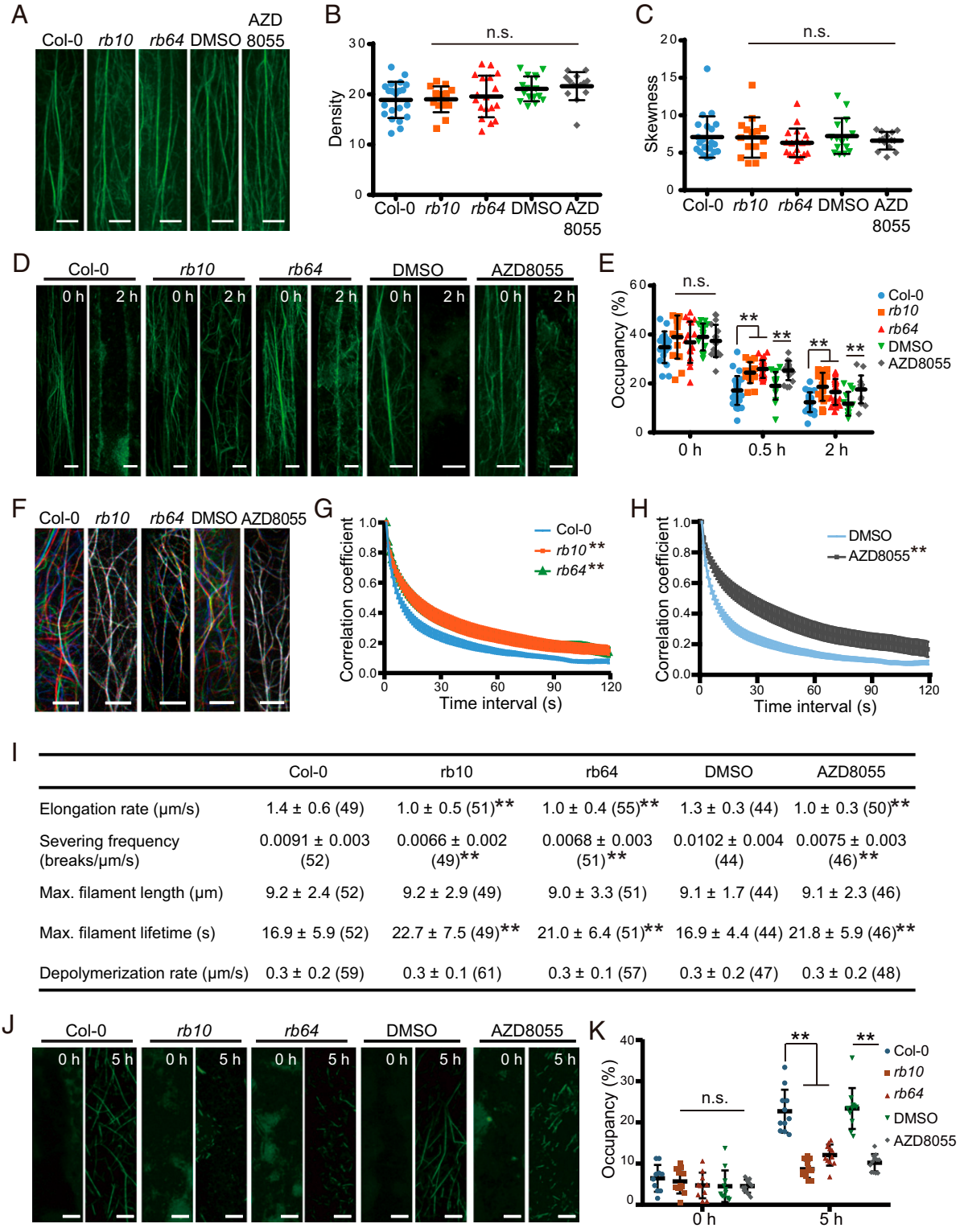

I

	Col-0	rb10	rb64	DMSO	AZD8055
Elongation rate (μm/s)	1.4 ± 0.6 (49)	1.0 ± 0.5 (51)**	1.0 ± 0.4 (55)**	1.3 ± 0.3 (44)	1.0 ± 0.3 (50)**
Severing frequency (breaks/μm/s)	0.0091 ± 0.003 (52)	0.0066 ± 0.002 (49)**	0.0068 ± 0.003 (51)**	0.0102 ± 0.004 (44)	0.0075 ± 0.003 (46)**
Max. filament length (μm)	9.2 ± 2.4 (52)	9.2 ± 2.9 (49)	9.0 ± 3.3 (51)	9.1 ± 1.7 (44)	9.1 ± 2.3 (46)
Max. filament lifetime (s)	16.9 ± 5.9 (52)	22.7 ± 7.5 (49)**	21.0 ± 6.4 (51)**	16.9 ± 4.4 (44)	21.8 ± 5.9 (46)**
Depolymerization rate (μm/s)	0.3 ± 0.2 (59)	0.3 ± 0.1 (61)	0.3 ± 0.1 (57)	0.3 ± 0.2 (47)	0.3 ± 0.2 (48)

Fig. 2. Impairment of TORC1 functions reduced actin filament dynamics. (*A*) Representative images showing mNeonGreen-fABD2-labeled actin cytoskeleton organization in hypocotyl epidermal cells of 3-d-old etiolated WT, *rb10*, *rb64*, DMSO-treated WT, and AZD8055-treated WT seedlings. Scale bars, 10 μm. (*B* and *C*) Quantification of density (*B*) and skewness (*C*) of actin filaments imaged as in (*A*). (*D*) Representative images showing mNeonGreen-fABD2-labeled actin cytoskeleton organization before and after 2-h LatB treatment in WT, *rb10*, *rb64*, DMSO-treated WT, and AZD8055-treated WT seedlings. Scale bars, 10 μm. (*E*) Quantification of actin filament occupancy in the cells after LatB treatment for different times. (*F*) Representative merged images showing mNeonGreen-fABD2-labeled actin filaments at 3 time points at 15-s intervals as separate colors (red, green, and blue) in WT, *rb10*, *rb64*, DMSO-treated WT, and AZD8055-treated WT seedlings. The white color indicates that actin filaments are present at the same region throughout the time series. Scale bar, 5 μm. (*G* and *H*) Correlation coefficient was calculated at all possible temporal intervals for time-lapse images of actin filaments in *rb* mutants (*G*) and AZD8055-treated WT seedlings (*H*). Values are means ± SEs ($n \geq 15$ cells from 5 seedlings per genotype). (*I*) Quantification of single actin filament dynamics in WT, *rb10*, *rb64*, DMSO-treated WT, and AZD8055-treated WT seedlings. Values are means ± SDs, with (*n*) = number of filaments in parentheses. (*J*) Representative images showing mNeonGreen-fABD2-labeled actin cytoskeleton organization before and after washing out LatB in WT, *rb10*, *rb64*, DMSO-treated WT, and AZD8055-treated WT seedlings. A high concentration of LatB (10 μM) was applied to completely depolymerize actin filaments before transferring the seedlings to water without or with AZD8055 for 5 h. Scale bars, 10 μm. (*K*) Quantification of actin filament occupancy in cells imaged as in (*J*). The double asterisk indicates significant difference from the control by Student's *t* test (*B*, *C*, *E*, *I*, and *K*) or one-way ANOVA (*G* and *H*); $^{**}P < 0.01$; n.s., not significant. The values from AZD8055-treated samples were compared to DMSO-treated samples for the statistical analysis.

Golgi, *trans*-Golgi network (TGN), and late endosome markers into the GFP-RAPTOR1B line, respectively. In addition, we stained the GFP-RAPTOR1B line with a mitochondria dye, MitoTracker, to investigate the possible colocalization of GFP-RAPTOR1B with mitochondria. The dual-labeled seedlings showed that GFP-RAPTOR1B did not colocalize well with the *trans*-Golgi marker sialyltransferase (ST)-RFP; the *cis*-Golgi marker SYP32-mCherry; the TGN markers vacuolar ATPase subunit a1 (VHAa1)-RFP and SYP61-CFP; or the late endosome markers RabF2a-mCherry, RabF2b-mCherry, RabC1-mCherry, and RabA1g-mCherry (Fig. 3*A*–*H*). Instead, GFP-RAPTOR1B and mNeonGreen-RAPTOR1B showed substantial colocalization with MitoTracker-labeled mitochondria (Fig. 3*I* and *SI Appendix*, Fig. S5*F*). High-resolution imaging further revealed that the GFP-RAPTOR1B mainly localized at the periphery of mitochondria (Fig. 3*J*–*L*). In line with these observations, immuno-transmission electron microscopy (TEM) experiments showed that the labeling of GFP-RAPTOR1B, quantified as gold particles per unit area, was significantly increased in the mitochondria and cytoplasm of the complementation lines compared to the Col-0 plants (Fig. 3*M*–*P*). In contrast, similar nonspecific signal was detected in the cell wall of both genotypes (Fig. 3*P*). Altogether, these data indicate that a portion of GFP-RAPTOR1B is localized to mitochondria in plant cells.

Inhibition of TORC1 Functions Leads to Reduced ATP Levels in Plant Cells. The localization of GFP-RAPTOR1B at mitochondria prompted us to analyze whether TORC1 regulated ATP production, which is important for actin filament turnover, in plant cells. The quantification of ATP concentration revealed that the ATP content was significantly reduced in *rb* mutants and in seedlings treated with TOR inhibitor AZD8055, as compared to their controls (Fig. 4*A* and *B*). Consistently, the FRET efficiency of the ATP biosensor, ATeam1.03-nD/nA (39), was significantly decreased by exogenous application of AZD8055 and the positive control for ATP synthesis inhibition, oligomycin, an inhibitor specific for the mitochondrial ATP synthase at low concentrations [up to 25 μM (40)], indicating a decline in ATP content after treatment with these inhibitors (Fig. 4*C* and *D*). Mitochondrial membrane potential drives the generation of ATP by mitochondria (41). In agreement with the low ATP content, the membrane potential, assessed by the fluorescent dyes rhodamine123 (Rho123) and tetramethylrhodamine methyl ester (TMRM), was significantly decreased in *rb* mutants and AZD8055-treated seedlings as compared to their controls (Fig. 4*E*–*L*). These data indicate an essential role of TORC1 in controlling physiological ATP production in plant cells.

The reduced ATP levels in TORC1-impaired plants prompted us to speculate that myosin-based organelle movement, which is ATP dependent, may also be inhibited in these plants. To assess this hypothesis, the mobility of ST-RFP-labeled Golgi, which relies on functional myosin XI (42), was quantified after the treatment with AZD8055. Application of AZD8055 significantly reduced the velocity of Golgi stacks compared to the control (*SI Appendix*, Fig. S6*A*). We then tested whether the reduced LatB sensitivity caused by AZD8055 treatment was dependent on myosin XI. For this purpose, a triple mutant of *myosin xi-k/1/2* (42) was grown on media supplemented with LatB in the absence or presence of AZD8055. Quantification of the ratios of hypocotyl length reduction showed that the triple mutant was less sensitive to LatB in the absence of AZD8055, resulting in decreased hypocotyl length reduction in the mutant compared to the Col-0 plants (*SI Appendix*, Fig. S6*B*). These observations were in accordance with the stabilized actin cytoskeleton in the mutant (43). Application of AZD8055 further decreased LatB sensitivity in the triple mutant as it did in WT plants (*SI Appendix*, Fig. S6*B*), indicating that the three myosin XIs were not required for the effects of AZD8055 on the actin cytoskeleton.

Actin Filaments Display Reduced Dynamics in ATP-Deficient Conditions. The formation of actin filaments from monomers represents a process consuming high levels of ATP (4). Given the reduced levels of ATP in the TORC1-impaired seedlings, we asked whether altered ATP levels affected the actin cytoskeleton in plant cells. For this purpose, we used three mitochondrial inhibitors, including oligomycin, the mitochondrial electron transport inhibitor antimycin A (AA), and the mitochondria uncoupler carbonyl cyanide m-chlorophenyl hydrazone (CCCP) and applied them to etiolated seedlings. Application of LatB markedly reduced the length of etiolated hypocotyls in a dose-dependent manner (Fig. 5*A* and *B*) and effectively depolymerized actin filaments, labeled by mNeonGreen-fABD2, in hypocotyl epidermal cells (Fig. 5*C* and *D*). However, when combined with mitochondrial inhibitors, the effects of LatB were substantially diminished, resulting in the decreased reduction in hypocotyl length and increased amounts of actin filaments remaining in the cells after LatB treatment (Fig. 5*A*–*D*). These data suggested that seedlings became less sensitive to LatB in the presence of the mitochondrial inhibitors.

We next determined whether inhibition of mitochondrial functions can affect actin filament organization and dynamics. The application of mitochondrial inhibitors did not cause obvious alteration of actin filament organization compared to the dimethyl sulfoxide (DMSO)–treated plants (*SI Appendix*, Fig. S7*A*–*C*). However, correlation coefficient analysis revealed that global actin filament dynamics was significantly inhibited in the presence of oligomycin compared to the control (Fig. 5*E* and *F*). Quantification of individual actin filament dynamics further demonstrated that actin filament elongation rate and severing frequency were significantly reduced, resulting in the increased lifetime of actin filaments in oligomycin-treated plants compared to the control (Fig. 5*G*). The washout experiment also revealed a significantly slower assembly of actin filaments in mitochondrial inhibitor–treated plants compared to the control (Fig. 5*H* and *I*). Altogether, these data demonstrated that the inhibition of mitochondrial functions led to phenotypes mimicking those observed in *TORC1*-impaired seedlings at both plant growth and actin dynamics levels.

TOR activity is inhibited by the application of mitochondrial inhibitors, including AA and CCCP (32, 44), and in mutants of *ise3* and *reptin*, which are likely defective in mitochondrial oxidative phosphorylation and ATP sensing, respectively (45). It was therefore possible that the effect of mitochondrial inhibitors on actin filament dynamics is due to the inactivation of TOR. To test this possibility, oligomycin was applied to *rb* mutants, AZD8055-treated plants, and the inducible *TOR-RNAi* mutants (32, 33). The application of oligomycin caused an additional decrease in ATP levels in all of the TORC1-defective plants (Fig. 5*J* and *SI Appendix*, Fig. S8*A*). The hypocotyl length reduction caused by LatB (Fig. 5*K* and *L* and *SI Appendix*, Fig. S8*B* and *C*) and actin filament dynamics (Fig. 5*M* and *N*) was also significantly reduced by oligomycin treatment in these plants compared to the control. These data hinted that inhibiting mitochondrial ATP synthesis affected actin dynamics by reducing ATP levels independently of the effect on TORC1.

Exogenous Feeding of Adenine Partially Recovers Actin Dynamics in *raptor1b* Mutants. To further explore the role of ATP in the reduced actin dynamics of TORC1-impaired

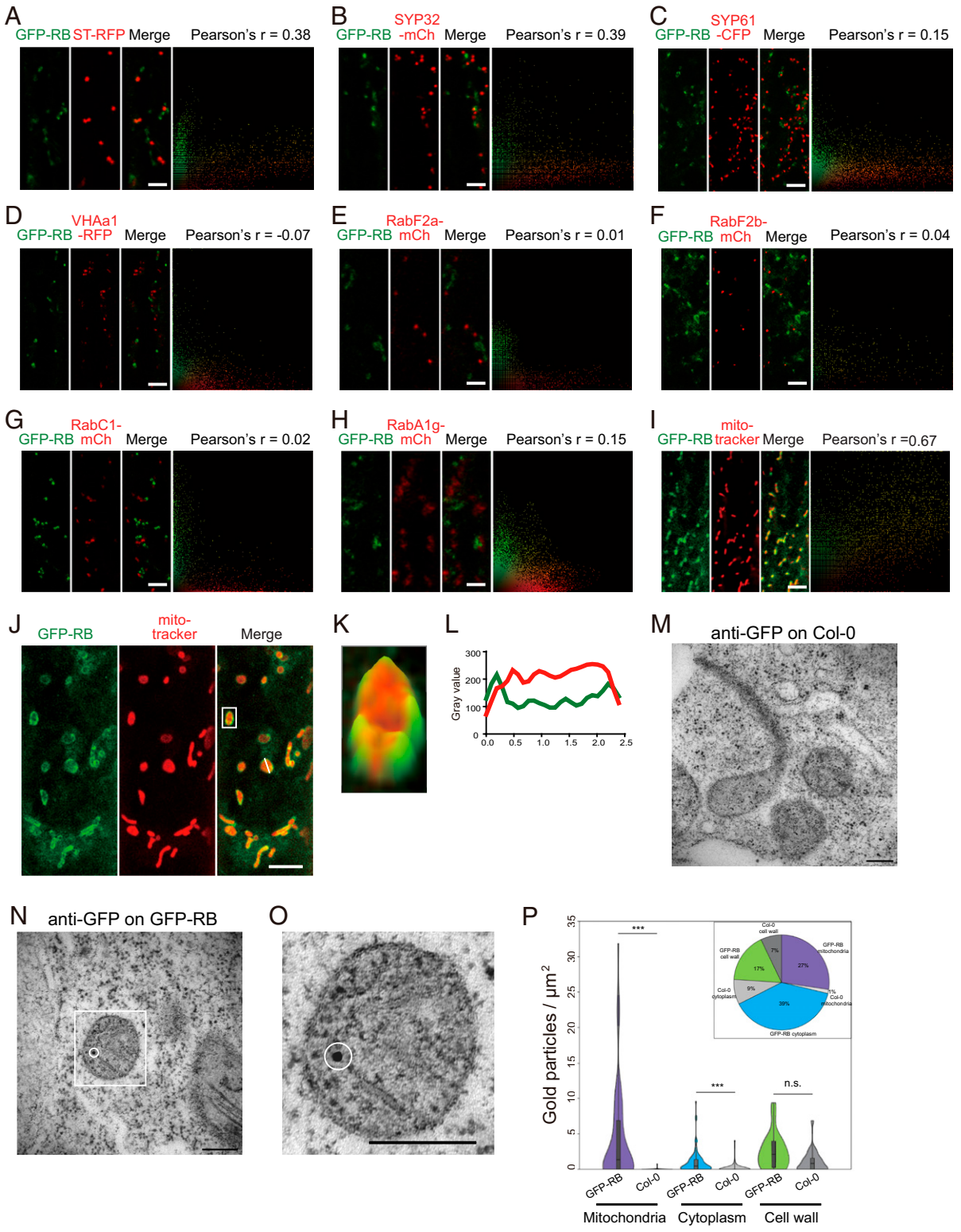

Fig. 3. GFP-RAPTOR1B can localize to the cytosol and mitochondria surface. (*A*–*H*) Representative images of 3-d-old etiolated hypocotyl cells expressing EGFP-RAPTOR1B (GFP-RB) and the Golgi markers ST-RFP (*A*) or SYP32-mCherry (*B*), GFP-RB, and the TGN markers, SYP61-CFP (*C*) or VHAa1-RFP (*D*), GFP-RB, and the late endosome/prevacuolar compartment markers, RabF2a-mCherry (*E*) or RabF2b-mCherry (*F*), GFP-RB, and the post-Golgi/endosomal marker RabC1-mCherry (*G*), GFP-RB, and the endosomal/recycling endosome marker RabA1g-mCherry (*H*). Scale bars in (*A*) to (*H*), 5 µm. (*I*) Representative images of GFP-RB and the mitochondrial dye MitoTracker. Scale bar, 5 µm. (*J*) High-resolution images of GFP-RB and MitoTracker. Scale bar, 5 µm. (*K*) Three-dimensional (3D) heatmap renderings of the fluorescence intensity of the GFP-RB and MitoTracker (white rectangle in *J*). (*L*) Relative fluorescent signal intensity across transect in (*J*). (*M*) Representative immuno-TEM image showing no immunolabeling with anti-GFP in the mitochondria of Col-0 hypocotyls. Scale bar, 200 nm. (*N*) Representative image of anti-GFP immunolabeling (white circle) in the mitochondria of GFP-RB hypocotyls. Scale bar, 200 nm. (*O*) Close-up of the mitochondria enclosed by white rectangles in (*N*). (*P*) Quantification of the number of gold particles per unit area (µm^2) in mitochondria, cytoplasm, and cell wall of GFP-RB and Col-0 hypocotyls. A total of 159 and 123 regions of interest were analyzed for GFP-RB and Col-0, respectively. Comparisons between GFP-RB and Col-0 for each compartment are performed with one-way ANOVA post hoc Dunn's test; ***$P < 0.001$; n.s., not significant. Inset: Percentage of all gold particles counted between mitochondria, cytoplasm, and cell wall regions of interest between GFP-RB and Col-0.

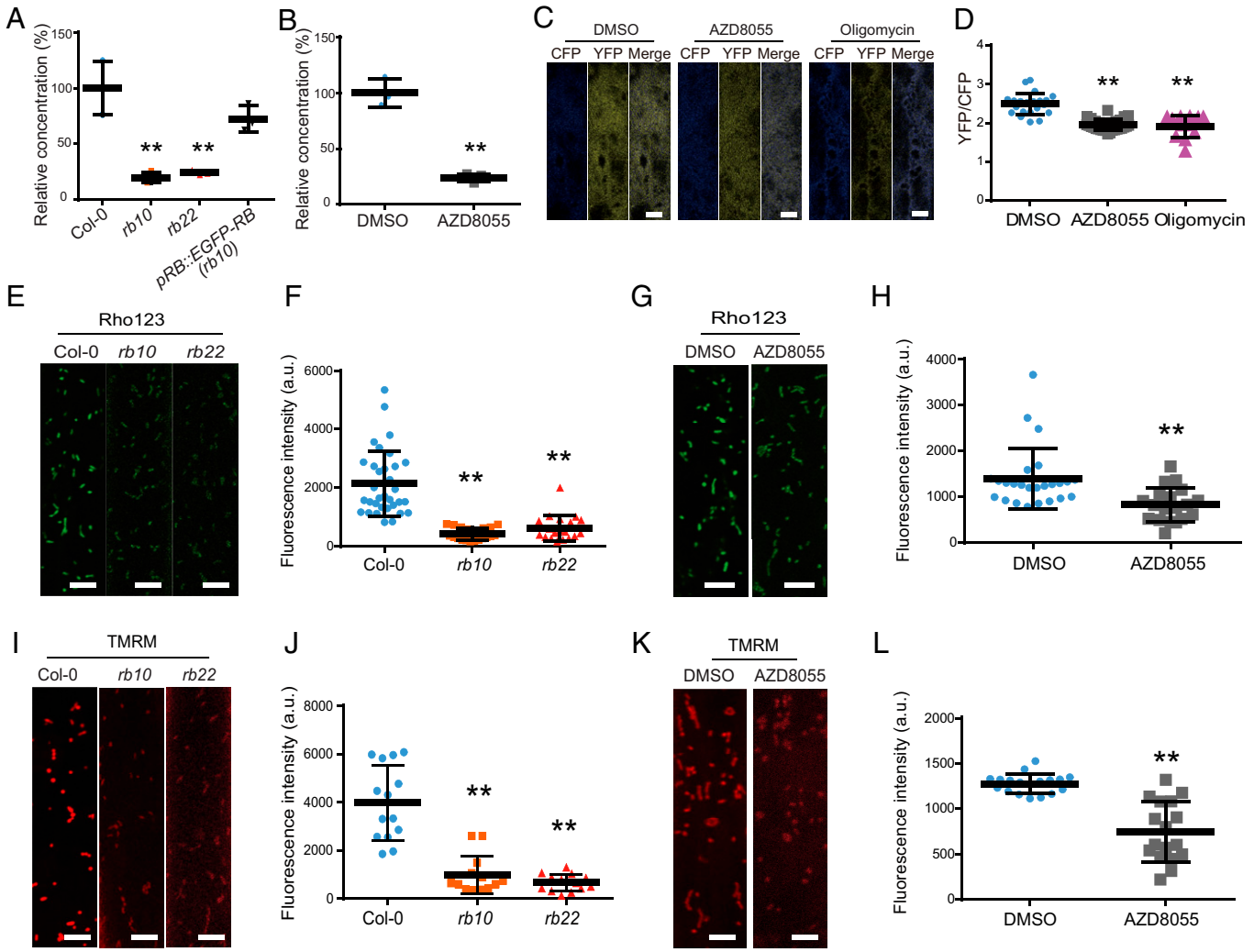

Fig. 4. Impairment of TORC1 functions reduced ATP levels. (*A*) Quantification of ATP concentration in 6-d-old dark grown WT, *raptor1b* mutants (*rb10*, *rb22*) and the complementation line in *rb10* background (*pRB::EGFP-RB* (*rb10*)). (*B*) Quantification of ATP concentration in 6-d-old etiolated WT seedlings grown on media without or with AZD8055. (*C*) Ratiometric imaging of ATP biosensor ATeam1.03-nD/nA in hypocotyl cells of 3-d-old etiolated seedlings grown on media with AZD8055 or oligomycin. Scale bars, 5 μm. (*D*) Quantification of YFP:CFP ratio in cells imaged as in (*C*). (*E*) Representative images of mitochondria stained with the MMP probe Rho123 in 3-d-old etiolated WT and *raptor1b* mutants. Scale bars, 5 μm. (*F*) Quantification of Rho123 fluorescent intensity in cells imaged as in (*E*). (*G*) Representative images of mitochondria stained with Rho123 in 3-d-old etiolated WT seedlings grown on media without or with AZD8055. Scale bars, 5 μm. (*H*) Quantification of Rho123 fluorescent intensity in cells imaged as in (*G*). (*I*) Representative images of mitochondria stained with MMP dye TMRM in 3-d-old etiolated WT and *raptor1b* mutants. Scale bars, 5 μm. (*J*) Quantification of TMRM fluorescent intensity in cells imaged as in (*I*). (*K*) Representative images of mitochondria stained with TMRM in 3-d-old etiolated WT seedlings grown on media without or with AZD8055. Scale bars, 5 μm. (*L*) Quantification of TMRM fluorescent intensity in cells imaged as in (*K*). The double asterisk indicates significant difference from control value by Student's *t* test; $^{**}P < 0.01$.

plants, these plants were supplied with a low concentration of exogenous adenine. Previous studies have demonstrated that adenine can stimulate ATP synthesis in plant cells, among other effects on core metabolism (38, 46, 47). Exogenous feeding of adenine did significantly elevate ATP levels (Fig. 6*A* and *SI Appendix*, Fig. S8*D*) and also restored LatB sensitivity (Fig. 6*B–E* and *SI Appendix*, Fig. S8*E* and *F*) of the *rb* mutants, AZD8055-treated plants, and the inducible *TOR-RNAi* mutants. More important, the overall actin filament dynamics, as evaluated by the correlation coefficient analysis, were significantly increased in *rb* mutans and AZD8055-treated plant cells by the application of adenine (Fig. 6*F–I*). The single actin filament dynamics, including the filament elongation rate, the filament severing frequency, and the filament lifetime, were also partially restored in *rb* mutants after the exogenous feeding of adenine (Fig. 6*J*). These results together support that adenine can restore actin filament dynamics, most likely by increasing ATP levels, in TORC1-compromised cells.

Discussion

The actin cytoskeleton forms a complex and dynamic network in eukaryotic cells, where they serve as tracks for vesicle transportation and organelle movement and positioning (48). How these actin networks are organized and how they remodel in the cytoplasm have been an area of intense scrutiny. An array of actin binding proteins has been uncovered to spatiotemporally regulate actin organization and dynamics (49). Here, we report that energy status provides a basis for actin dynamics in plant cells.

In the epidermal cells of *Arabidopsis* etiolated hypocotyls, cortical actin arrays display incredibly rapid elongation rates, which are among the fastest recorded in eukaryotic cells (7, 8, 50). By contrast, actin filament depolymerization is very rare and occurs at rates that are much slower than the filament elongation rates (7, 8). Instead, the rapid filament elongation is balanced by filament disassembly through stochastic severing (7, 8). Our data

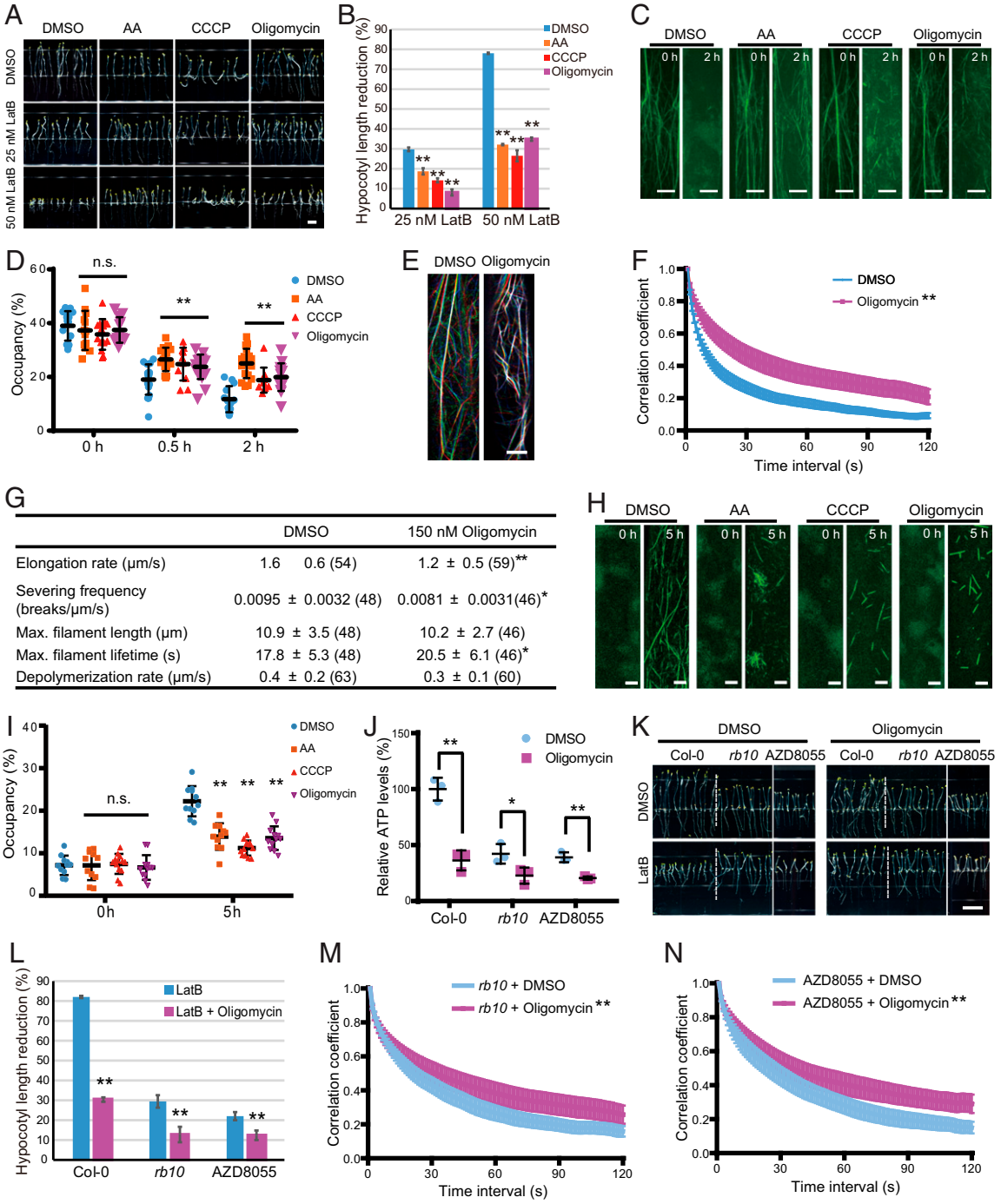

Fig. 5. Inhibition of mitochondrial function reduced plant sensitivity to actin cytoskeleton inhibitor and actin filament dynamics. (*A*) Six-day-old Col-0 seedlings grown in the dark on half MS media supplemented with increasing concentration of LatB in the absence or presence of mitochondrial blockers AA, CCCP, or oligomycin. Scale bar, 5 mm. (*B*) Bar graphs showing the ratios of hypocotyl length reduction caused by LatB treatment imaged as in (*A*). Values are means ± SEs from 3 biological replicates with more than 10 seedlings per replicate. (*C*) Representative images showing mNeonGreen-fABD2-labeled actin cytoskeleton before and after 2-h LatB treatment in the absence or presence of mitochondrial blocker. Scale bars, 10 μm. (*D*) Quantification of actin filament occupancy in the cells imaged as in (*C*). (*E*) Representative merged images showing mNeonGreen-fABD2-labeled actin filaments at 3 time points at 15-s intervals as separate colors (red, green, and blue) in DMSO- or oligomycin-treated WT seedlings. The white color indicates that actin filaments are present at the same region throughout the time series. Scale bar, 5 μm. (*F*) Correlation coefficient was calculated at all possible temporal intervals for time-lapse images of actin filaments in DMSO- or oligomycin-treated WT seedlings. Values are means ± SEs ($n \geq 15$ cells from 5 seedlings per genotype). (*G*) Quantification of single actin filament dynamics in the absence or presence of oligomycin. Values are means ± SDs, with (n) = number of filaments in parentheses. (*H*) Representative images showing mNeonGreen-fABD2-labeled actin cytoskeleton before and after washing out LatB in the absence or presence of mitochondrial blocker. A high concentration of LatB (10 μM) was applied to completely depolymerize actin filaments before transferring the seedlings to water without or with mitochondrial blocker. Scale bars, 10 μm. (*I*) Quantification of actin filament occupancy in the cells imaged as in (*H*). (*J*) Quantification of ATP levels in WT, *rb10*, and AZD8055-treated WT plants grown on media with DMSO or oligomycin. (*K*) Six-day-old WT, *rb10*, and AZD8055-treated WT plants grown in the dark on half MS media supplemented with DMSO or LatB in the presence or absence of oligomycin. Scale bar, 10 mm. (*L*) Bar graphs showing the ratios of hypocotyl length reduction caused by LatB treatment as shown in (*K*). Values are means ± SEs from 3 biological replicates with more than 10 seedlings per replicate. (*M* and *N*) Correlation coefficient analysis of global actin filament dynamics in *rb10* mutants (*M*) and AZD8055-treated WT seedlings (*N*) grown on media supplemented with DMSO or oligomycin. Values are means ± SEs ($n \geq 15$ cells from 5 seedlings per genotype). In (*B*) and (*L*), the samples treated with LatB were normalized to samples treated with DMSO, while the samples treated with a combination of mitochondrial inhibitors and LatB were normalized to samples treated with mitochondrial inhibitors alone. Single and double asterisks indicate significant difference from control value by Student's *t* test (*B*, *D*, *G*, *I*, *J*, and *L*) or one-way ANOVA (*F*, *M*, *N*); *$P < 0.05$; **$P < 0.01$; n.s., not significant.

revealed that in cells with decreased ATP levels, either caused by the inhibition of mitochondrial functions or by the repression of TORC1 functions, actin filaments became less dynamic and less sensitive to the disassembly caused by LatB treatment. Consistently, the quantification of single actin filament dynamics revealed that both the elongation rate and the severing frequency of actin filaments were dramatically reduced, which resulted in long-lived actin filaments in the ATP-deficient cells. Intriguingly, the alteration of actin dynamics did not significantly affect actin organization, suggesting that a new balance between actin filament assembly and disassembly was established. Because ATP is critical for actin polymerization, it is not unexpected that reduced ATP levels slow actin polymerization. It is likely that reduced ATP levels lead to a shift in abundance of ADP-G-actin versus ATP-G-actin. The polymerization rate of ADP-G-actin is significantly slower than ATP-G-actin (51, 52), which could account for the decreased actin polymerization rate observed in the ATP-deficient cells. In contrast, it is unlikely that ATP levels directly influence actin filament severing. One possible scenario would be that alteration of the cytosolic ATP content modulated the activity of actin-binding proteins. One such candidate would be ADF/cofilin proteins, which mediate actin cytoskeletal alterations in porcine kidney cultured cells under ATP-depleted conditions (53). Whether ADF proteins and other actin-binding proteins function in modulating actin dynamics in plant cells during ATP depletion still requires further investigation.

The biological significance of reducing actin dynamics under ATP-deficient conditions is obvious. Hydrolysis of actin-ATP has been considered to be a major energy drain (4). It was estimated in a nucleotide-exchange study that up to 50% of total ATP use of resting platelets is required merely to maintain the actin network (54). Slowing actin filament turnover could spare up to 50% of the ATP consumed by all neuronal processes (4). Reduced actin dynamics, such as those observed in ATP-deficient plant cells in this study, therefore, could limit ATP consumption. Saving this energy, while still retaining actin organization, may be important for plant cells to maintain the processes that are essential for long-term survival during ATP-deficient conditions. It could also be beneficial for plant cells to restore growth by using the existing cytoskeleton with minimal ATP cost while ATP levels are being recovered.

Similar reduced actin dynamics have also been observed in energy-deprived yeast and mammalian cells (55). Under nutrient-rich and growth-promoting conditions, actin filaments and cables are actively assembled and disassembled in yeast, with entire actin architecture reconstructions occurring in approximately one to two minutes (56). By contrast, upon acute glucose starvation, which causes a drop in ATP levels in yeast, actin cables are highly stabilized and become resistant to disassembly in the presence of high concentration of latrunculin A (LatA) (55). Similarly, actin filaments and bundles in ATP-depleted HeLa cells are stable and show a reduced sensitivity to LatA treatment (55). Thus, our work, together with previous findings, suggest that the inhibition of actin dynamics may present a conserved response to energy stress in eukaryotic cells. As TOR is an evolutionarily conserved signal hub for energy status in cells (20, 31), it is possible that the reduced actin dynamics caused by energy deficiency in yeast and mammalian cells is also regulated by TOR.

A recent work reported that both actin filament bundling and TOR activities were enhanced in *ipms1* mutants with elevated levels of BCAAs, as well as in WT plants fed with exogenous BCAAs (28). The effects of BCAA overaccumulation on actin reorganization are compromised in TOR-silencing cells, but not in *raptor1b* mutants, suggesting that TOR, but not RAPTOR, is required for BCAA-induced actin filament bundling (28). Our work revealed that both TOR and RAPTOR are involved in the regulation of actin filament dynamics, but not organization, in etiolated seedlings. Together, these studies support the important roles of TOR in modulating multiple aspects of the actin cytoskeleton in plants and suggest that TOR may regulate the actin cytoskeleton via distinct mechanisms, depending on external conditions. Indeed, although our data support that TOR controls ATP levels to regulate actin cytoskeleton, other mechanisms could not be excluded. The inhibition of TOR activity by applying its specific inhibitor, Torin2, decreases the phosphorylation of two actin-binding proteins, VILLIN2 and VILLIN3, in *Arabidopsis* seedlings (57). TOR can directly bind to ROP2, which is a well-known upstream regulator of the actin cytoskeleton in plants (35, 58). These studies hint that TOR may also modulate actin cytoskeleton through VILLINs and ROP-based signaling pathway.

Diverse subcellular localizations have been reported for TOR in plant cells, including the localization in cytoplasm and nucleus when transiently expressed in onion epidermal cells (59), diffuse distribution at the periphery of cytoplasm when transiently expressed in *Nicotiana benthamiana* epidermal cells (58), and localization at endosome when activated by ROP2 in *N. benthamiana* (58). Through a transient expression system, TOR cofactor LST8 is shown to localize at endosomes labeled by RabC1 in *Arabidopsis* cotyledons (19). However, these studies are based on transient transformation and overexpression studies of TOR, or related components, and little is therefore known about the subcellular localization of TOR and thus where the TORC1 works in plant cells. In this report, we carefully evaluate the subcellular localization of functional GFP-RAPTOR1B and mNeonGreen-RAPTOR1B, and observe at least two distinct pools of RAPTOR1B, cytosolic RAPTOR1B and mitochondrial RAPTOR1B. These observations, together with the data that ATP levels and mitochondrial membrane potential are reduced in *raptor1b* mutants and AZD8055-treated plants, establish a physical and functional link between TORC1 and mitochondria in plant cells. However, further studies are needed to uncover the mechanism underlying the control of mitochondrial functions by plant TORC1. It has been well documented that mammalian TOR (mTOR) complex 1 (mTORC1) indirectly stimulates mitochondrial functions by modulating the transcription of mitochondrial nuclear-encoded genes as well as control of the translation of nuclear-encoded mitochondrial mRNAs such as mitochondrial ribosomal proteins and components of complexes I and V (60–63). In plants, the inhibition of TOR activity widely suppresses, at both transcription and translation levels, the expression of mitochondrial ribosomal proteins (57). These studies support the possibility that controlling the expression of mitochondrial proteins may represent a common way for the regulation of mitochondrial functions by both mammalian and plant TORC1. Alternatively, various observations indicate that mTORC2 is linked to mitochondria in mammalian cells. A large portion of mTOR localizes in close proximity to the outer mitochondrial membrane (64). mTOR forms a complex with the mitochondrial outer-membrane protein Bcl-xl and VDAC1 and can phosphorylate Bcl-xl in vitro (65). mTORC2 is localized to the mitochondria-associated endoplasmic reticulum membrane (MAM), where the complex regulates mitochondrial physiology by phosphorylating MAM resident proteins (66). It is therefore also possible that the mitochondrial-localized plant TORC1 directly interacts and phosphorylates proteins on or near mitochondria to achieve its impact on mitochondria.

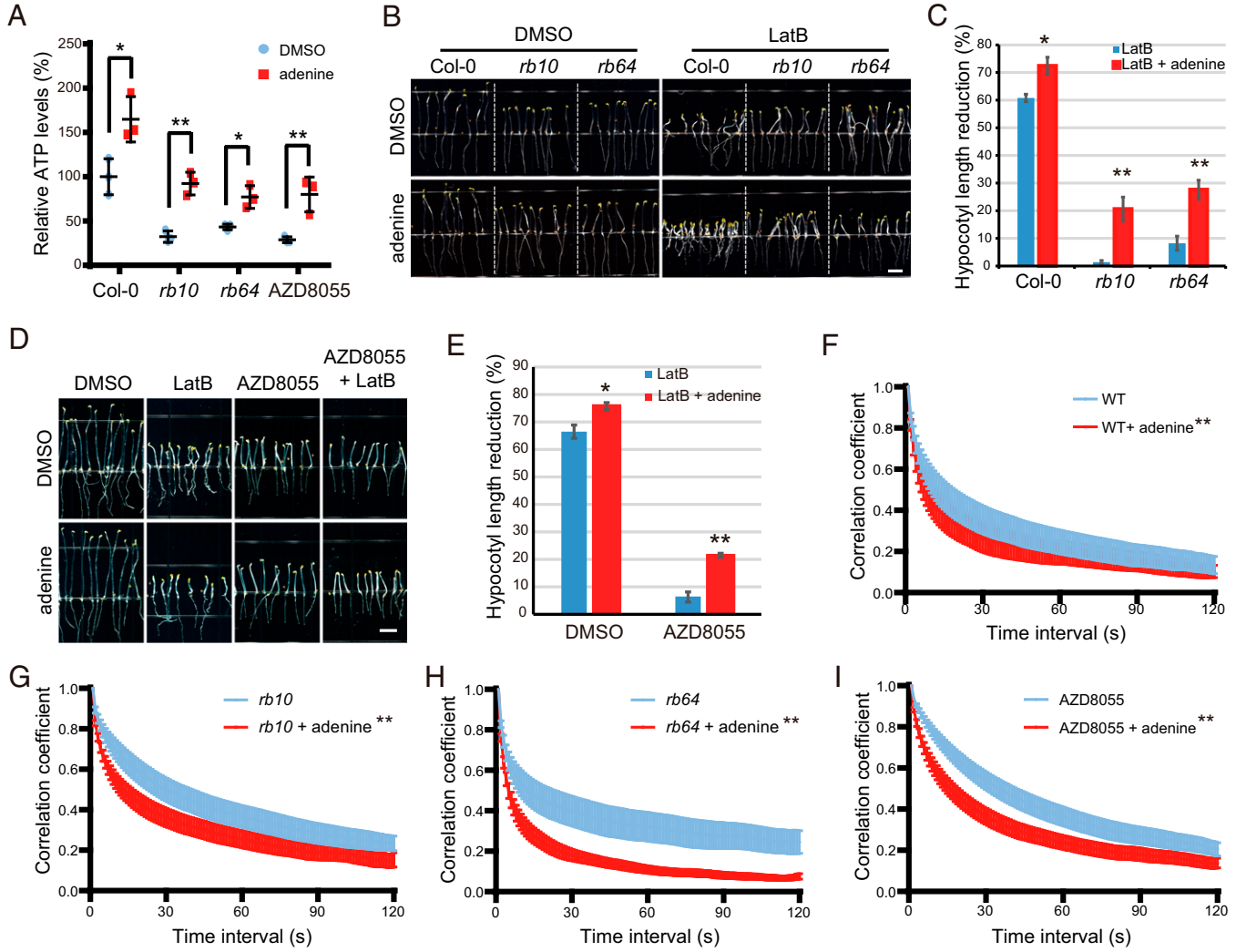

J

	Control	Control (adenine)	*rb10*	*rb10* (adenine)	*rb64*	*rb64* (adenine)
Elongation rate (μm/s)	1.4 ± 0.6 (49)	1.4 ± 0.5 (54)	1.0 ± 0.5 (51)	1.2 ± 0.3 (56)*	1.0 ± 0.4 (55)	1.2 ± 0.3 (53)*
Severing frequency (breaks/μm/s)	0.0091 ± 0.003 (52)	0.0140 ± 0.006 (50)**	0.0066 ± 0.002 (49)	0.0106 ± 0.004 (50)**	0.0068 ± 0.003 (51)	0.0105 ± 0.004 (50)**
Max. filament length (μm)	9.2 ± 2.4 (52)	7.8 ± 2.5 (50)*	9.2 ± 2.9 (49)	8.2 ± 1.8 (50)	9.0 ± 3.3 (51)	8.1 ± 2.0 (50)
Max. filament lifetime (s)	16.9 ± 5.9 (52)	14.7 ± 4.6 (50)*	22.7 ± 7.5 (49)	15.0 ± 4.0 (50)**	21.0 ± 6.4 (51)	16.0 ± 5.1 (50)**
Depolymerization rate (μm/s)	0.3 ± 0.2 (59)	0.3 ± 0.1 (51)	0.3 ± 0.1 (61)	0.3 ± 0.1 (55)	0.3 ±0.1 (57)	0.3 ± 0.1 (52)

Fig. 6. Exogenous feeding of adenine partially restored sensitivity to LatB and actin filament dynamics in TORC1-impaired plants. (*A*) Quantification of ATP levels in WT, *rb* mutants, and AZD8055-treated WT plants grown on media supplemented with DMSO or adenine. (*B*) Six-day-old seedlings grown in the dark on half MS media supplemented with DMSO or LatB in the absence or presence of adenine. Scale bar, 5 mm. (*C*) Bar graphs show the ratios of hypocotyl length reduction induced by LatB as shown in (*B*). The samples treated with LatB were normalized to samples treated with DMSO, while the samples treated with a combination of adenine and LatB (LatB + adenine) were normalized to samples treated with adenine alone. Values are means ± SEs from 3 biological replicates with more than 10 seedlings per replicate. (*D*) Six-day-old seedlings grown in the dark on half MS media supplemented with DMSO, AZD8055, and/or LatB in the absence or presence of adenine. Scale bar, 5 mm. (*E*) Bar graphs show the ratios of hypocotyl length reduction induced by LatB as shown in (*D*). Values are means ± SEs from 3 biological replicates with more than 10 seedlings per replicate. (*F–I*) Correlation coefficient analysis of global actin filament dynamics in WT (*F*), *rb10* (*G*), *rb64* (*H*), and AZD8055-treated WT (*I*) seedlings grown on media supplemented with DMSO or adenine. Values are means ± SEs ($n \geq 15$ cells from 5 seedlings per genotype). (*J*) Quantification of single actin filament dynamics in WT and *rb* mutants grown on media supplemented with adenine. Values are means ± SDs, with (n) = number of filaments in parentheses. Values from the adenine group were compared with the control group of the same genotype for the statistical analysis. Single and double asterisks indicate significant difference from control value by Student's *t* test (*A*, *C*, *E*, and *J*) or one-way ANOVA (*F–I*); *$P < 0.05$; **$P < 0.01$.

In plants, the TOR signaling pathway is activated by sugar (glucose and sucrose), nucleotides, diverse hormones, and some amino acids (28, 32, 36, 67–69). In *Arabidopsis* seedlings at the photoautotrophic transition checkpoint, glucose can quickly activate TOR protein kinase, which is indispensable for young seedlings to exit from the mitotic quiescent state at both the transcript and

cellular levels and for subsequent cell division and growth (32). The activation of TOR by glucose depends on functional glycolysis and mitochondrial electron transport chain, as the application of glycolysis inhibitor (2-DG) and mitochondrial blockers (AA, 2,4-dinitrophenol, CCCP) prevent TOR activation by glucose (32, 44). This notion is further validated by genetic evidence that TOR activity is reduced in the mutant defective in mitochondrial oxidative phosphorylation (*ise3*) and the mutant likely defective in ATP sensing (*reptin*) (45). In this study we reveal that the TORC can positively regulate the function of mitochondria and control ATP levels in plant cells. Thus, our data, together with previous reports, suggest a positive feedback loop in TOR-mediated regulation of energy metabolism. A recent work reported that several amino acids, including Ile and Gln, could activate the TOR signaling pathway, which subsequently inhibits the mitochondrial respiratory pathways consuming amino acids as fuel in mature leaves (67). It is possible that the effect of TOR complex on mitochondrial function is different between tissue, developmental stages, and external conditions.

Materials and Methods

Plant Materials and Growth Conditions. *Arabidopsis* seedlings were grown on vertical plates containing half-strength Murashige and Skoog (half MS) media supplemented with 1% sucrose and 0.5% Gelzan (Sigma-Aldrich, G1910) at 22 °C. For chemical treatment, the dose for individual inhibitors was selected to achieve one-third to two-thirds reduction of hypocotyl length. Information about cloning of constructs, generation of transgenic plants, and the primers used in this study can be found in the *SI Appendix, Supplementary Materials and Methods* and Table S1.

ATP Concentration and Mitochondrial Membrane Potential Detection. ATP concentration was quantified using the ATP Colorimetric/Fluorometric Assay Kit (Sigma-Aldrich, FLAA). The mitochondrial membrane potential (MMP) of mitochondria was measured with Rho123 (Sigma-Aldrich, R8004) or TMRM (Sigma-Aldrich, T5428).

Fluorescence Resonance Energy Transfer (FRET) Imaging and Analysis: ATeam 1.03-nD/nA. ATeam1.03-nD/nA fluorescence was excited at 458 nm and the emission signals were detected at 470 to 507 nm (Em463–507, CFP image) and 526 to 561 nm (Em524–544, YFP image), respectively. Fluorescence intensities were measured using ImageJ software, and the YFP:CFP ratio was calculated as the FRET efficiency (39).

Colocalization Analysis. For labeling mitochondria, seedlings were stained with MitoTracker (Invitrogen, M7512). The subcellular localization of GFP-, RFP-, mCherry-, or CFP-tagged proteins were obtained from 3-d-old etiolated hypocotyls with a spinning-disk confocal microscope (UltraView VoX, PerkinElmer).

Visualization and Quantification of Actin Filament Organization and Dynamics. Fluorescent images of mNeoGreen-fABD2 were obtained from epidermal cells in 3-d-old etiolated hypocotyls. The percentage of occupancy (density) and extent of bundling (skewness) of actin filaments were quantified using the density and skewness plugins, respectively, in ImageJ (37, 70). The stochastic dynamic parameters and the correlation coefficient were analyzed as previously described (8, 38).

Immuno-TEM. Hypocotyl tissues near the apical hook of 3-d-old etiolated seedling were dissected for immuno-TEM. A negative control with no primary antibody was included for immunolocalization and imaging. For quantification, 159 and 123 regions of interest were analyzed from GFP-RB and Col-0, respectively, from 3 biological replicates per genotype.

Statistical Analysis. The statistical analysis was performed using Student's *t* test or one-way ANOVA.

Data, Materials, and Software Availability. All of the study data are included in the article and/or the *SI Appendix*.

ACKNOWLEDGMENTS. We acknowledge the Experimental Technology Center for Life Sciences, Beijing Normal University, and are grateful to Dr. Xiaoyan Zhang for technical support. We thank Prof. Markus Schwarzlander (University of Münster) for the ATeam1.03-nD/nA line, Prof. Yan Xiong (Fujian Agriculture and Forestry University) for the *tor-es* lines and the anti-S6K antibody, and Prof. Yuling Jiao (Peking University) for support in the protoplast transformation experiment. This work was supported by the National Natural Science Foundation of China (32070194 and 31870174 to Y.Z., and 32100279 to T.W.). S.P. acknowledges the financial aid from ARC Discovery (DP19001941), Villum Investigator (Project ID: 25915), DNRF Chair (DNRF155), and Novo Nordisk Laureate (NNF19OC0056076) grants. H.E.M. acknowledges funding from the Canada Research Chairs program (Canada Research Chair in Plant Cell Biology) and a Canadian Natural Sciences and Engineering Council Discovery Grant (NSERC DG 2020-05959).

Author affiliations: [a]Key Laboratory of Cell Proliferation and Regulation Biology of Ministry of Education, College of Life Science, Beijing Normal University, Beijing 100875, China; [b]Martin-Luther-University Halle-Wittenberg, Institute of Plant Physiology, 06120 Halle (Saale), Germany; [c]Department of Cell & Systems Biology, University of Toronto, Toronto, ON M5S 3G5, Canada; [d]State Key Laboratory of Conservation and Utilization of Bio-resources in Yunnan, Center for Life Sciences, School of Life Sciences, Yunnan University, Kunming 650091, China; [e]School of Biosciences, University of Melbourne, Parkville 3010 VIC, Melbourne, Australia; [f]School of Natural Sciences, University of Tasmania, Hobart 7001, TAS, Australia; [g]Metabolomics Core Facility, Max Planck Institute for Biology of Ageing, 50931 Cologne, Germany; [h]Department of Plant and Environmental Sciences, University of Copenhagen, 1871 Frederiksberg C, Denmark; [i]Copenhagen Plant Science Center, University of Copenhagen, 1871 Frederiksberg C, Denmark; [j]Joint International Research Laboratory of Metabolic & Developmental Sciences, State Key Laboratory of Hybrid Rice, SJTU-University of Adelaide Joint Centre for Agriculture and Health, School of Life Sciences and Biotechnology, Shanghai Jiao Tong University, Shanghai 200240, China; and [k]Max-Planck Institute for Molecular Plant Physiology, Am Muehlenberg 1, 14476 Potsdam, Germany

1. M. M. Klosinska, C. A. Crutchfield, P. H. Bradley, J. D. Rabinowitz, J. R. Broach, Yeast cells can access distinct quiescent states. *Genes Dev.* **25**, 336–349 (2011).
2. T. D. Pollard, J. A. Cooper, Actin, a central player in cell shape and movement. *Science* **326**, 1208–1212 (2009).
3. P. J. Hussey, T. Ketelaar, M. J. Deeks, Control of the actin cytoskeleton in plant cell growth. *Annu. Rev. Plant Biol.* **57**, 109–125 (2006).
4. B. W. Bernstein, J. R. Bamburg, Actin-ATP hydrolysis is a major energy drain for neurons. *J. Neurosci.* **23**, 1–6 (2003).
5. S. Buracco, S. Claydon, R. Insall, Control of actin dynamics during cell motility. *F1000 Res.* **8**, 1977 (2019).
6. R. Dominguez, K. C. Holmes, Actin structure and function. *Annu. Rev. Biophys.* **40**, 169–186 (2011).
7. J. L. Henty-Ridilla, J. Li, L. Blanchoin, C. J. Staiger, Actin dynamics in the cortical array of plant cells. *Curr. Opin. Plant Biol.* **16**, 678–687 (2013).
8. C. J. Staiger *et al.*, Actin filament dynamics are dominated by rapid growth and severing activity in the Arabidopsis cortical array. *J. Cell Biol.* **184**, 269–280 (2009).
9. J. Li, L. Blanchoin, C. J. Staiger, Signaling to actin stochastic dynamics. *Annu. Rev. Plant Biol.* **66**, 415–440 (2015).
10. S. Wullschleger, R. Loewith, M. N. Hall, TOR signaling in growth and metabolism. *Cell* **124**, 471–484 (2006).
11. R. Zoncu, A. Efeyan, D. M. Sabatini, mTOR: From growth signal integration to cancer, diabetes and ageing. *Nat. Rev. Mol. Cell Biol.* **12**, 21–35 (2011).
12. T. Dobrenel *et al.*, TOR signaling and nutrient sensing. *Annu. Rev. Plant Biol.* **67**, 261–285 (2016).
13. R. A. Saxton, D. M. Sabatini, mTOR signaling in growth, metabolism, and disease. *Cell* **168**, 960–976 (2017).
14. A. González, M. N. Hall, Nutrient sensing and TOR signaling in yeast and mammals. *EMBO J.* **36**, 397–408 (2017).
15. R. Loewith *et al.*, Two TOR complexes, only one of which is rapamycin sensitive, have distinct roles in cell growth control. *Mol. Cell* **10**, 457–468 (2002).
16. E. Jacinto *et al.*, Mammalian TOR complex 2 controls the actin cytoskeleton and is rapamycin insensitive. *Nat. Cell Biol.* **6**, 1122–1128 (2004).
17. B. Menand *et al.*, Expression and disruption of the Arabidopsis TOR (target of rapamycin) gene. *Proc. Natl. Acad. Sci. U.S.A.* **99**, 6422–6427 (2002).
18. G. H. Anderson, B. Veit, M. R. Hanson, The Arabidopsis AtRaptor genes are essential for post-embryonic plant growth. *BMC Biol.* **3**, 12 (2005).
19. M. Moreau *et al.*, Mutations in the Arabidopsis homolog of LST8/GβL, a partner of the target of rapamycin kinase, impair plant growth, flowering, and metabolic adaptation to long days. *Plant Cell* **24**, 463–481 (2012).
20. L. Shi, Y. Wu, J. Sheen, TOR signaling in plants: Conservation and innovation. *Development* **145**, 1–13 (2018).
21. H. Tatebe, K. Shiozaki, Evolutionary conservation of the components in the TOR signaling pathways. *Biomolecules* **7**, 77 (2017).
22. J. O. Brunkard, Exaptive evolution of target of rapamycin signaling in multicellular eukaryotes. *Dev. Cell* **54**, 142–155 (2020).
23. D. Deprost *et al.*, The Arabidopsis TOR kinase links plant growth, yield, stress resistance and mRNA translation. *EMBO Rep.* **8**, 864–870 (2007).

24. M. A. Salem *et al.*, RAPTOR controls developmental growth transitions by altering the hormonal and metabolic balance. *Plant Physiol.* **177**, 565–593 (2018).
25. Y. Zhang *et al.*, Inhibition of TOR represses nutrient consumption, which improves greening after extended periods of etiolation. *Plant Physiol.* **178**, 101–117 (2018).
26. D. Rispal *et al.*, Target of rapamycin complex 2 regulates actin polarization and endocytosis via multiple pathways. *J. Biol. Chem.* **290**, 14963–14978 (2015).
27. J. Xie, X. Wang, C. G. Proud, Who does TORC2 talk to? *Biochem. J.* **475**, 1721–1738 (2018).
28. P. Cao *et al.*, Homeostasis of branched-chain amino acids is critical for the activity of TOR signaling in *Arabidopsis*. *eLife* **8**, 1–24 (2019).
29. R. C. O'Malley, J. R. Ecker, Linking genotype to phenotype using the Arabidopsis unimutant collection. *Plant J.* **61**, 928–940 (2010).
30. M. A. Salem, Y. Li, A. Wiszniewski, P. Giavalisco, Regulatory-associated protein of TOR (RAPTOR) alters the hormonal and metabolic composition of Arabidopsis seeds, controlling seed morphology, viability and germination potential. *Plant J.* **92**, 525–545 (2017).
31. Y. Xiong, J. Sheen, The role of target of rapamycin signaling networks in plant growth and metabolism. *Plant Physiol.* **164**, 499–512 (2014).
32. Y. Xiong *et al.*, Glucose-TOR signalling reprograms the transcriptome and activates meristems. *Nature* **496**, 181–186 (2013).
33. Y. Xiong, J. Sheen, Rapamycin and glucose-target of rapamycin (TOR) protein signaling in plants. *J. Biol. Chem.* **287**, 2836–2842 (2012).
34. P. Wang *et al.*, Reciprocal regulation of the TOR kinase and ABA receptor balances plant growth and stress response. *Mol. Cell* **69**, 100–112.e6 (2018).
35. X. Li *et al.*, Differential TOR activation and cell proliferation in *Arabidopsis* root and shoot apexes. *Proc. Natl. Acad. Sci. U.S.A.* **114**, 2765–2770 (2017).
36. M. H. Montané, B. Menand, ATP-competitive mTOR kinase inhibitors delay plant growth by triggering early differentiation of meristematic cells but no developmental patterning change. *J. Exp. Bot.* **64**, 4361–4374 (2013).
37. T. Higaki, N. Kutsuna, T. Sano, N. Kondo, S. Hasezawa, Quantification and cluster analysis of actin cytoskeletal structures in plant cells: Role of actin bundling in stomatal movement during diurnal cycles in Arabidopsis guard cells. *Plant J.* **61**, 156–165 (2010).
38. L. Vidali *et al.*, Myosin XI is essential for tip growth in Physcomitrella patens. *Plant Cell* **22**, 1868–1882 (2010).
39. V. De Col *et al.*, ATP sensing in living plant cells reveals tissue gradients and stress dynamics of energy physiology. *eLife* **6**, 1–29 (2017).
40. S. Krömer, M. Stitt, H. W. Heldt, Mitochondrial oxidative phosphorylation participating in photosynthetic metabolism of a leaf cell. *FEBS Lett.* **226**, 352–356 (1988).
41. L. D. Zorova *et al.*, Mitochondrial membrane potential. *Anal. Biochem.* **552**, 50–59 (2018).
42. V. V. Peremyslov, A. I. Prokhnevsky, V. V. Dolja, Class XI myosins are required for development, cell expansion, and F-actin organization in Arabidopsis. *Plant Cell* **22**, 1883–1897 (2010).
43. C. Cai, J. L. Henty-Ridilla, D. B. Szymanski, C. J. Staiger, Arabidopsis myosin XI: A motor rules the tracks. *Plant Physiol.* **166**, 1359–1370 (2014).
44. N. Zhang *et al.*, Metabolite-mediated TOR signaling regulates the circadian clock in *Arabidopsis*. *Proc. Natl. Acad. Sci. U.S.A.* **116**, 25395–25397 (2019).
45. J. O. Brunkard *et al.*, TOR dynamically regulates plant cell-cell transport. *Proc. Natl. Acad. Sci. U.S.A.* **117**, 5049–5058 (2020).
46. E. Gout, F. Rébeillé, R. Douce, R. Bligny, Interplay of Mg^{2+}, ADP, and ATP in the cytosol and mitochondria: Unravelling the role of Mg^{2+} in cell respiration. *Proc. Natl. Acad. Sci. U.S.A.* **111**, E4560–E4567 (2014).
47. I. Loef, M. Stitt, P. Geigenberger, Increased levels of adenine nucleotides modify the interaction between starch synthesis and respiration when adenine is supplied to discs from growing potato tubers. *Planta* **212**, 782–791 (2001).
48. K. Rottner, J. Faix, S. Bogdan, S. Linder, E. Kerkhoff, Actin assembly mechanisms at a glance. *J. Cell Sci.* **130**, 3427–3435 (2017).
49. T. D. Pollard, Actin and actin-binding proteins. *Cold Spring Harb. Perspect. Biol.* **8**, a018226 (2016).
50. A. P. Smertenko, M. J. Deeks, P. J. Hussey, Strategies of actin reorganisation in plant cells. *J. Cell Sci.* **123**, 3019–3028 (2010).
51. I. Fujiwara, D. Vavylonis, T. D. Pollard, Polymerization kinetics of ADP- and ADP-Pi-actin determined by fluorescence microscopy. *Proc. Natl. Acad. Sci. U.S.A.* **104**, 8827–8832 (2007).
52. T. D. Pollard, Rate constants for the reactions of ATP- and ADP-actin with the ends of actin filaments. *J. Cell Biol.* **103**, 2747–2754 (1986).
53. S. L. Ashworth *et al.*, ADF/cofilin mediates actin cytoskeletal alterations in LLC-PK cells during ATP depletion. *Am. J. Physiol. Renal Physiol.* **284**, F852–F862 (2003).
54. J. L. Daniel, I. R. Molish, L. Robkin, H. Holmsen, Nucleotide exchange between cytosolic ATP and F-actin-bound ADP may be a major energy-utilizing process in unstimulated platelets. *Eur. J. Biochem.* **156**, 677–684 (1986).
55. L. Xu, A. Bretscher, Rapid glucose depletion immobilizes active myosin V on stabilized actin cables. *Curr. Biol.* **24**, 2471–2479 (2014).
56. J. B. Moseley, B. L. Goode, The yeast actin cytoskeleton: From cellular function to biochemical mechanism. *Microbiol. Mol. Biol. Rev.* **70**, 605–645 (2006).
57. M. R. Scarpin, S. Leiboff, J. O. Brunkard, Parallel global profiling of plant TOR dynamics reveals a conserved role for LARP1 in translation. *eLife* **9**, e58795 (2020).
58. M. Schepetilnikov *et al.*, GTPase ROP2 binds and promotes activation of target of rapamycin, TOR, in response to auxin. *EMBO J.* **36**, 886–903 (2017).
59. M. Ren *et al.*, Target of rapamycin regulates development and ribosomal RNA expression through kinase domain in Arabidopsis. *Plant Physiol.* **155**, 1367–1382 (2011).
60. M. Morita *et al.*, mTOR coordinates protein synthesis, mitochondrial activity and proliferation. *Cell Cycle* **14**, 473–480 (2015).
61. M. Morita *et al.*, mTORC1 controls mitochondrial activity and biogenesis through 4E-BP-dependent translational regulation. *Cell Metab.* **18**, 698–711 (2013).
62. J. T. Cunningham *et al.*, mTOR controls mitochondrial oxidative function through a YY1-PGC-1alpha transcriptional complex. *Nature* **450**, 736–740 (2007).
63. I. Ben-Sahra, G. Hoxhaj, S. J. H. Ricoult, J. M. Asara, B. D. Manning, mTORC1 induces purine synthesis through control of the mitochondrial tetrahydrofolate cycle. *Science* **351**, 728–733 (2016).
64. B. N. Desai, B. R. Myers, S. L. Schreiber, FKBP12-rapamycin-associated protein associates with mitochondria and senses osmotic stress via mitochondrial dysfunction. *Proc. Natl. Acad. Sci. U.S.A.* **99**, 4319–4324 (2002).
65. A. Ramanathan, S. L. Schreiber, Direct control of mitochondrial function by mTOR. *Proc. Natl. Acad. Sci. U.S.A.* **106**, 22229–22232 (2009).
66. C. Betz *et al.*, Feature article: mTOR complex 2-Akt signaling at mitochondria-associated endoplasmic reticulum membranes (MAM) regulates mitochondrial physiology. *Proc. Natl. Acad. Sci. U.S.A.* **110**, 12526–12534 (2013).
67. B. M. O'Leary, G. G. K. Oh, C. P. Lee, A. H. Millar, Metabolite regulatory interactions control plant respiratory metabolism via target of rapamycin (TOR) kinase activation. *Plant Cell* **32**, 666–682 (2020).
68. M. Busche, M. R. Scarpin, R. Hnasko, J. O. Brunkard, TOR coordinates nucleotide availability with ribosome biogenesis in plants. *Plant Cell* **33**, 1615–1632 (2021).
69. Z. Kazibwe, J. Soto-Burgos, G. C. MacIntosh, D. C. Bassham, TOR mediates the autophagy response to altered nucleotide homeostasis in an RNase mutant. *J. Exp. Bot.* **71**, 6907–6920 (2020).
70. J. L. Henty *et al.*, Arabidopsis actin depolymerizing factor4 modulates the stochastic dynamic behavior of actin filaments in the cortical array of epidermal cells. *Plant Cell* **23**, 3711–3726 (2011).